



HAL
open science

Advanced characterization of the structuration of ionic liquids in a copolyester

Benjamin Megevand, Sébastien Pruvost, Jannick Duchet-Rumeau

► **To cite this version:**

Benjamin Megevand, Sébastien Pruvost, Jannick Duchet-Rumeau. Advanced characterization of the structuration of ionic liquids in a copolyester. *European Polymer Journal*, 2019, 118, pp.97 - 106. 10.1016/j.eurpolymj.2019.05.030 . hal-03484516

HAL Id: hal-03484516

<https://hal.science/hal-03484516>

Submitted on 20 Dec 2021

HAL is a multi-disciplinary open access archive for the deposit and dissemination of scientific research documents, whether they are published or not. The documents may come from teaching and research institutions in France or abroad, or from public or private research centers.

L'archive ouverte pluridisciplinaire **HAL**, est destinée au dépôt et à la diffusion de documents scientifiques de niveau recherche, publiés ou non, émanant des établissements d'enseignement et de recherche français ou étrangers, des laboratoires publics ou privés.



Distributed under a Creative Commons Attribution - NonCommercial 4.0 International License

Advanced characterization of the structuration of ionic liquids in a copolyester

Benjamin Megevand, Sébastien Pruvost,* Jannick Duchet-Rumeau*

*Université de Lyon, INSA Lyon, UMR CNRS 5223, IMP Ingénierie des Matériaux Polymères, F-69621
Villeurbanne, France*

* *E-mail : sebastien.pruvost@insa-lyon.fr; jannick.duchet@insa-lyon.fr*

Abstract

The influence of the addition in small amounts (2wt%) of two phosphonium-based ionic liquids (ILs) on the nanostructuration and mechanical properties of a poly(butylene-adipate-co-terephthalate) (PBAT) matrix was investigated using complementary approaches. Dielectric spectroscopy and nanomechanical characterizations using atomic force microscopy (Peak-Force QNM mode, Bruker) were used along X-ray diffraction, differential scanning calorimetry and dynamic mechanical analysis to explain the mechanical (tensile) properties of each system. The semicrystalline matrix was found to have a spherulitic structure, with crystalline lamellae composed of butylene terephthalate units. In one case, the addition of an immiscible phosphonium-phosphinate ionic liquid (il-TMP) to the matrix, inducing a 33% increase of the strain at break, was found via AFM to induce a nodular microstructure with dissipative effects and smooth nodule-matrix interphases. In the other case, a phosphonium-chloride ionic liquid (il-Cl), being miscible in the amorphous phases, increases the chain mobility of the mobile amorphous fraction (MAF) consisting of free polymer chains, while it hinders the relaxation, thus chain movements, of the confined rigid amorphous fraction (RAF). This double effect induced a moderate macroscopic Young's modulus drop (less than -20%) with a +60% increase of the strain at break, and no significant influence on thermal properties. AFM *in situ* mechanical measurements, along with dielectric spectroscopy, allowed to propose complete mechanisms for the ILs-matrix interactions, highlighting the potential of such additives for the tuning of the properties of polymers.

Keywords:

AFM, Dielectric spectroscopy, PBAT, Copolyester, Ionic liquids, Nanomechanics

1. Introduction

In polymer science, developing ways to design, tailor and adjust properties of existing materials is a major challenge. The main routes to modify such properties are via the processing of the polymer, by acting on its physical structuration and/or on phenomena such as phase separation, or via the formulation with additives, adding physical or chemical interactions that can modify the final properties.

The use of ionic liquids (ILs) represents a novel route to modify the structure and properties of polymers[1]. The numerous existing cation-anion combinations make them suitable for various applications: they have been used as plasticizers[2, 3, 4], solvents for cellulose[5], intercalating agents for bio/nanocomposites with clays[6], compatibilizers for biopolymer blends[7], as well as reagents and parts of thermoset networks[8]. Ionic liquids have also shown promising capabilities for the nanostructuration of polymer systems such as fluorinated copolymers, in which a tunable effect on the crystallization behavior, on the dispersion morphology and on the crystalline phase structure have been reported by Yang *et al.*[9].

This has been particularly useful in the field of biopolymers, where the capability to modify the properties is a critical issue: in order to propose an alternative to traditional oil-based polymers, the goal is to be able to tune the properties of biopolymers to obtain materials that are equivalent.

A key to that issue is to understand completely the mechanisms that link formulations and processes to functional properties, at every scale of the material. Atomic Force Microscopy[10] is a particularly useful tool to investigate the properties of materials at nanoscale with an outstanding resolution, allowing to evidence phenomena such as nanostructuration, identifying features and patterns of few nanometers[11]. The intermittent contact of an extremely sharp tip with the sample surface allows to gather informations about its local properties[12], and the capability to acquire force curves[13, 14] led recently to the development of Peak-Force QNM (Bruker, USA), an AFM mode allowing a high-resolution mapping of mechanical properties of surfaces[15].

This has already allowed promising results for the understanding of the structure-properties links of polymers[16, 17]. The technique gives access to the mechanical behavior at a nanoscopic scale, by mapping properties such as the tip-sample adhesion force, the

local elastic modulus or the energy dissipation. A better understanding and visualization of various phenomena could be achieved, for instance the creation via annealing of an interphase between two blended immiscible polymers[18, 19, 20], or the surface properties changes due to surface treatments[21] or photo-oxidation[22]. AFM nanomechanical mappings recently gave encouraging results for the study of polymers–ionic liquids systems[23, 24].

In this study, the effects of some phosphonium–based ionic liquids on a biodegradable matrix are investigated. The poly(butylene-adipate-*co*-terephthalate) (PBAT) is an aliphatic-aromatic copolyester used in various forms, from films to fibers[25] in fields such as medicine, agriculture and food packaging[26]. The use of PBAT has been revealed to be very promising in fully biodegradable blends[27, 28] and composites[29]. In those particular fields, phosphonium ionic liquids have also already shown a good potential with PBAT, for their compatibilizing and/or intercalating properties to design nanocomposites with clays[30, 31], lignine[32] and blends with PLA[7, 33].

Given the wide field of applications of the PBAT/ILs combinations, it is proposed in the present work to go deeper in the characterization of their mutual interactions, choosing two ILs that are already known for their different behavior when blended with PBAT. As a starting point, it is chosen to focus on the modification of tensile mechanical properties induced by the addition of 2wt% of a ionic liquid, as reported by Livi *et al.*[34] and represented in Figure 1. The further analysis aims to explain, for both ionic liquid, its effect on the matrix to reach such modifications of mechanical properties: an increase of the strain at break, from 510% (neat PBAT) to 810% and 680% with il-Cl and il-TMP, respectively, and a modulus drop from 47 to 40 MPa with il-Cl.

AFM nanomechanical mappings already demonstrated their capabilities to highlight the link between structure and properties on both biopolymers[35, 36, 37] and polymer structures blended with ionic liquids[38, 33]. The combination of this technique with dielectric spectroscopy having shown promising results for polymer–based materials[39], it is used here to elucidate the interaction between PBAT and the ILs and propose an action mechanism.

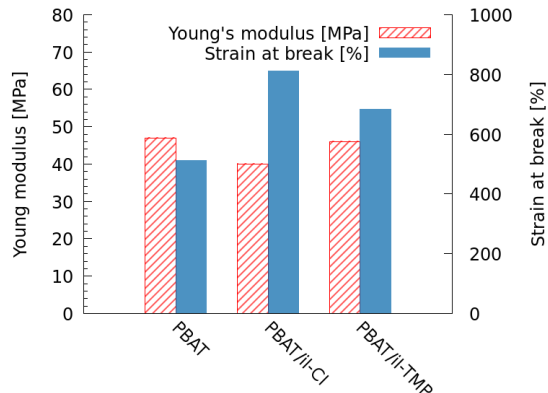


Figure 1: Tensile properties of the blends measured by Livi et al.[34]

2. Experimental

2.1. PBAT/ILs blends

Poly(butylene-adipate-co-terephthalate) (PBAT) was supplied by BASF Co. (Germany) under the trade name of Ecoflex®. It is a statistical copolymer with 50% butylene adipate (PBA) and 50% butylene terephthalate (PBT) segments.

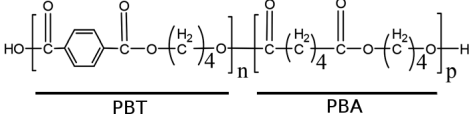
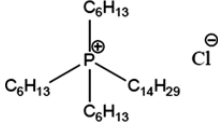
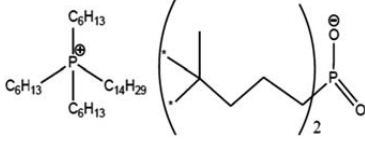
The two ionic liquids based on a trihexyltetradecyl phosphonium cation with two different anions (*i.e.* chloride denoted il-Cl and bis-2,4,4-(trimethylpentyl)phosphinate denoted il-TMP) were provided by Cytec Industries Inc. They are in a liquid state at ambient temperature and at any temperature range used in this study. The chemical structures of the matrix and ionic liquids are summarized in Table 1.

2.1.1. Processing of PBAT with and without ILs

All the samples used in this study were prepared by twin screw extrusion and injection molding, as a simple and scalable process. Ionic liquids were introduced in low amounts (2% wt) and the blends were processed at 160°C and 100 rpm with a 100 rpm rotation for about 3 minutes (the same was done for the neat PBAT matrix) using a 15 g-capacity DSM micro-extruder (Midi 2000 Heerlen, NL)[34].

Dielectric spectroscopy samples. The samples used for dielectric spectroscopy were injected into a 1 mm thick disk mold (diameter: 32.5 mm) at 60°C. Circular gold electrodes were

Table 1: Designation and structure of the components considered in this study

Nomenclature	Chemical Structure
<i>PBAT matrix:</i>	
	 <p style="text-align: center;"> PBT PBA </p>
<i>Ionic Liquids:</i>	
il-Cl	
il-TMP	

sputtered on both sides of the samples using a mask (diameter: 25 mm), applying 30 mA during 300 s for each side.

AFM, DMA and XRD samples. The samples used for DMA, XRD and AFM characterizations were obtained from dumbbell-shaped specimens, injected the same way as for the disks described above. For XRD, the wide extremities were used, while for AFM and DMA samples the center beam was preferred.

The surfaces for AFM mappings were prepared via microtomy at -130°C along the cross-section of the beams to get a smooth surface without affecting the microstructure.

2.1.2. Density measurements

Volumetric mass density measurements were performed using an hydrostatic weighing system provided by Mettler Toledo, used on a Mettler Toledo precision weighing scale. The samples are precisely weighed in air and in water, and the volumetric mass ρ_{sample} is given by equation 1. All the samples studied here have a higher density than water, so their weight in water can be measured.

$$\rho_{sample} = \frac{\rho_{water}}{1 - \frac{m_w}{m_{air}}} \quad (1)$$

Where ρ_{water} is the volumetric mass of water at room temperature (998.29 kg.m⁻³ at 20°C), m_w the weight of the sample in water and m_{air} the weight of the dry sample in air.

2.2. Atomic Force Microscopy

The AFM mappings were carried out using a Multimode 8 scanning probe microscope (Bruker, Santa Barbara, USA) with a Nanoscope V controller under ambient conditions. To map mechanical properties such as local modulus and adhesion forces, the PeakForce QNM mode (Quantitative NanoMechanics) was used. Mechanical properties such as adhesion force and local modulus could be mapped, by applying the Derjaguin-Müller-Toporov (DMT) contact theory to model the geometry and behavior of the tip-sample contact[40]. The Johnson-Kendall-Roberts model (JKR) could also be used[41], but the most relevant for polymers is a theoretical transitory model between JKR and DMT which is not numerically applicable[42, 43]. The JKR model is more adapted to a larger tip radius than those used in this study (20 to 30 nm in average) and to larger indentations (limited in this study to 5 nm, at least on the exploited data). The DMT model is implemented in the AFM software and, being relevant for the purpose of this study, it is chosen here. The contact modulus E^* is defined by equation 2.

$$\frac{1}{E^*} = \left(\frac{1 - \nu_1^2}{E_1} \right) + \left(\frac{1 - \nu_2^2}{E_2} \right) \quad (2)$$

where E_1 and E_2 represent the modulus of the silicon tip and of the sample surface, respectively, while ν_1 and ν_2 represent their respective Poisson's ratio. The DMT model predicts the relation given by equation 3, allowing to calculate mechanical properties at each pixel of an AFM image.

$$F = \frac{4}{3}E^*\sqrt{Rd^3} + F_{adh} \quad (3)$$

where F is the applied force, F_{adh} the adhesion force, R the tip radius, d the tip-sample distance and E^* the equivalent contact modulus.

The Al-coated¹ TAP150 probe with an aluminium coating was used (nominal spring

¹Some AFM probes are coated with aluminium to optimize the laser deflection.

constant: 5 N/m). Prior to each measurements session, the deflection sensitivity is measured on a hard sapphire surface, and the time synchronization parameters are fixed. The spring constant is calibrated using a thermal tuning method and the tip radius is evaluated using a reference sample of known modulus (amorphous and homogeneous polystyrene film), as suggested by the *relative calibration* method[15]. The local modulus is calculated using the part of the force–distance curves that corresponds to the withdrawal of the probe, that usually shows a cleaner linear behavior and more stable results.

2.3. X-ray diffraction

Wide angle X-Ray diffraction (WXR) analysis was carried out using a X-Ray diffractometer (D8 Advance, Bruker, USA) with a Cu radiation source operated at 40 kV and 40 mA.

The diffractograms were treated using Fityk (version 1.2.1)[44]. Each peak was fitted using a gaussian or pseudo-Voigt profile² to gather every parameter to apply Scherrer’s equation:

$$d = \frac{K\lambda}{\beta \cdot \cos(\theta)} \quad (4)$$

λ being the X-ray wavelength (for a copper source, $\lambda = 1.5418 \text{ \AA}$), β the full width at half maximum of the peak and θ being Bragg’s angle. K is a dimensionless factor linked to the shape of the crystallites. Its value for polybutylene terephthalate (PBT) is usually fixed at 0.89 or 0.9 by most authors[45, 46]. This value should only concern crystallites with a spherical shape, and other values were documented for each crystalline directions of simple crystallites shapes (*i.e.* cubic, octahedral and tetrahedral)[47]. The reported values for K are typically in the 0.7—2.0 range. Anyway, the PBT crystallizes with a triclinic unit cell[48, 49], and no clue of the exact crystalline shape is available. In this case, it is chosen to keep the value of 0.89 for K , as a first estimation, keeping in mind that the results for d can be under-estimated.

²The pseudo-Voigt fit was only used for the $\bar{1}01$ peak. See Table 2 and Figure 3.

2.4. Dynamic Mechanical Analysis (DMA)

Uniaxial torsion DMA was performed using Dynamic Mechanical Thermal Analyzer (Ares G2, TA Instruments, USA), at fixed frequency of 1 Hz and heating rate of 3°C/min using specimens of dimensions 25 mm×4 mm×2 mm in a temperature range of -80 to 80°C applying a 0.1% imposed strain.

2.5. Differential Scanning Calorimetry (DSC)

DSC measurements were performed using a Q20 (from TA Instruments, USA) from -70 to 170°C using a Chiller cooling system. The samples were kept for 2 min at 200°C to erase their thermal history before being cooled and then heated at a 10°C/min rate under a nitrogen flow (50 mL/min). The glass temperature (T_g) was measured at the maximum of the derivative of the heat flow signal when the glass transition step occurs, in the heating phase. The crystallinity χ_c of PBAT was calculated with the heat of melting of fully crystalline for PBAT, evaluated by Herrera *et al.* to be 114 $J.g^{-1}$.

2.6. Dielectric spectroscopy

The dielectric analysis measurements were carried out using a ModuLab XM system (Solartron analytical-AMETEK, USA). Each sample underwent two cycles with isothermal frequency sweeps from 10^6 to 10^{-2} Hz performed every 3°C from -70 to 60°C, applying a 5V – *RMS* voltage.

The results were analyzed using WinFit (Novocontrol, Germany). The transitions associated with relaxations or conductivity were fitted using Havriliak-Negami plots and the obtained fit parameters were used to calculate the activation energy. The Havriliak-Negami equation[50] stands:

$$\bar{\varepsilon}_r(f) = \varepsilon_\infty + \frac{\Delta\varepsilon}{(1 + (2\pi f\tau)^\alpha)^\beta} \quad (5)$$

where f is the frequency, $\bar{\varepsilon}_r(f)$ is the complex permittivity, ε_∞ the permittivity at infinite frequency, $\Delta\varepsilon = \varepsilon_0 - \varepsilon_\infty$ with ε_0 the permittivity at low frequency, and τ is the relaxation time of the material at the considered temperature. α and β are the Havriliak-Negami shape parameters and are comprised between 0 and 1. Adjusting those parameters to obtain a

proper fit of a relaxation allows, via the specific relaxation time τ at different temperatures, to calculate the activation energy E_A associated with it applying an Arrhenius law³, given in eqn 6.

$$\tau(T) = \tau_\infty \cdot \exp\left(\frac{-E_A}{k_B T}\right) \quad (6)$$

Where τ_∞ is a constant (relaxation time at an infinite temperature, in s), k_B the Boltzmann constant and T the temperature in Kelvins. The same equation stands replacing τ by σ_0 , the direct current (DC) conductivity (here measured at very low frequency, *i.e.* 0.01 Hz), to calculate the activation energy associated with the conduction phenomenon.

3. Results and discussion

3.1. Morphological and thermal characterization

3.1.1. Densities

The volumetric mass density was measured to be $1.217 \pm 0.001 \text{ g.cm}^{-3}$ for every sample. Since no significant change is observed, it can be considered that the macroscopical organization of the PBAT polymer chains remains unchanged by the presence of ionic liquids.

3.1.2. Microstructures

Figure 2 shows AFM micrographs of the microstructure of the three systems, with height and DMT modulus mappings. First, while il-Cl seems to be miscible in the PBAT matrix without changing its apparent structure, il-TMP forms nodules and is at least partially immiscible in PBAT. This is consistent with the morphologies observed in transmission electron microscopy by Livi *et al.*. The apparent holes in topographic images of the PBAT/il-TMP system and the fact that these features display a low modulus is also consistent with the idea of ionic liquid nodules.

The AFM DMT modulus images of the three blends also suggest a common crystalline organization in a lamellar form, creating spherulites at a larger scale. A more detailed view of

³All the measurements gave a linear relation between $\ln(\tau)$ and $1/T$, justifying the application of the Arrhenius law and not the VTF (Vogel-Fulcher-Tammann) law.

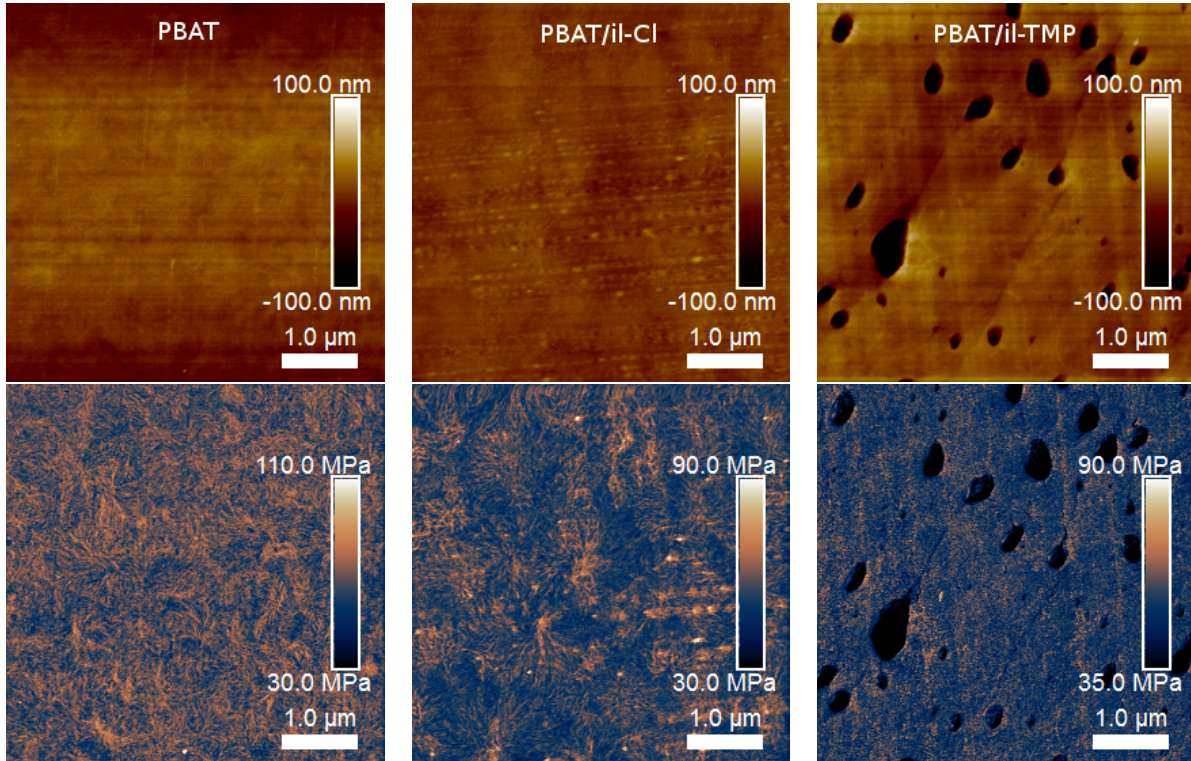


Figure 2: AFM height (top) and DMT Modulus (bottom) maps of a $5 \times 5 \mu\text{m}^2$ region of a: (left) PBAT sample; (center) PBAT/il-Cl sample; (right) PBAT/il-TMP sample

the lamellae in AFM is given further. DMT modulus images already proved their efficiency to identify and characterize crystalline lamellar structures[37].

3.1.3. Crystalline structure

The degree of crystallinity of the blends was measured to be $14 \pm 1\%$ in DSC for all the blends without significant difference due to the presence of ionic liquids. A XRD analysis was carried out, revealing the main peaks associated with the crystalline directions for the three systems, displayed in Figure 3.

The peaks correspond to those observed by Briber and Thomas for the PBT homopolymer[51]. The fact that the crystalline domains in PBAT are composed of PBT units is confirmed by Herrera *et al.*[52] and by Kuwabara[53].

To estimate the size of the corresponding crystallites, Scherrer's equation was applied to each peak. The results are summarized in Table 2.

Given the uncertainty associated to the peak fitting in XRD, due to the preponderance

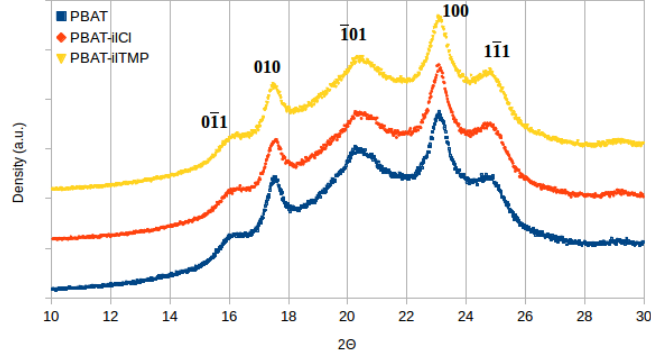


Figure 3: WAXS scans of neat PBAT and PBAT/ILs blends. Each peak corresponds to a PBT crystalline direction, according to the study of Briber and Thomas[51].

Table 2: Main PBT crystalline directions observed in the PBAT/ILs blends and corresponding estimated domain sizes obtained with the application of Scherrer’s equation (eqn 4).

	d [nm]				
Orientation	$0\bar{1}1$	010	$\bar{1}01$	100	$1\bar{1}1$
PBAT	8.1	13.5	3.0	10.3	6.5
PBAT/il-Cl	9.0	14.2	2.7	11.2	6.7
PBAT/il-TMP	7.4	12.4	3.7	9.3	5.9

of the amorphous phase, the difference in the sizes of the crystallites between the blends are irrelevant. It is thus considered that there is no major observable variation of the size of the crystallites caused by the ionic liquids. Such crystallites are observable in AFM, by scanning parts of the spherulites as in Figure 4.

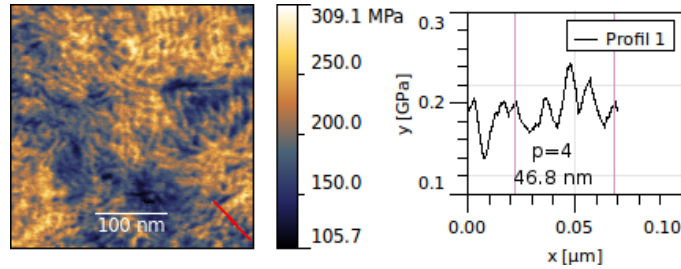


Figure 4: $350 \times 350\text{nm}$ AFM DMT modulus map of a PBAT surface exhibiting crystalline lamellae, and corresponding modulus profile taken along the red line, perpendicularly to the direction of the lamellae. Crystalline lammelae correspond to the modulus peaks.

A red profile is drawn perpendicularly to the lamellae, and 4 modulus peaks (corresponding to stiff PBT crystallites) are identifiable between the purple vertical lines (representing a distance of 46.8 nm). This means an average spacing of less than 12 nm between the lamellae in this case, of the same order of magnitude as their estimated dimensions given in Table 2. This suggests that the amorphous chains stacked between lamellae are quite confined, as confirmed further.

3.1.4. Thermomechanical relaxations

The DMA analysis was carried out on the blends to identify the thermal transitions of the three systems. The evolution of the storage modulus and of the loss modulus across the temperature range (-80 to 80°C) is shown in Figure 5.

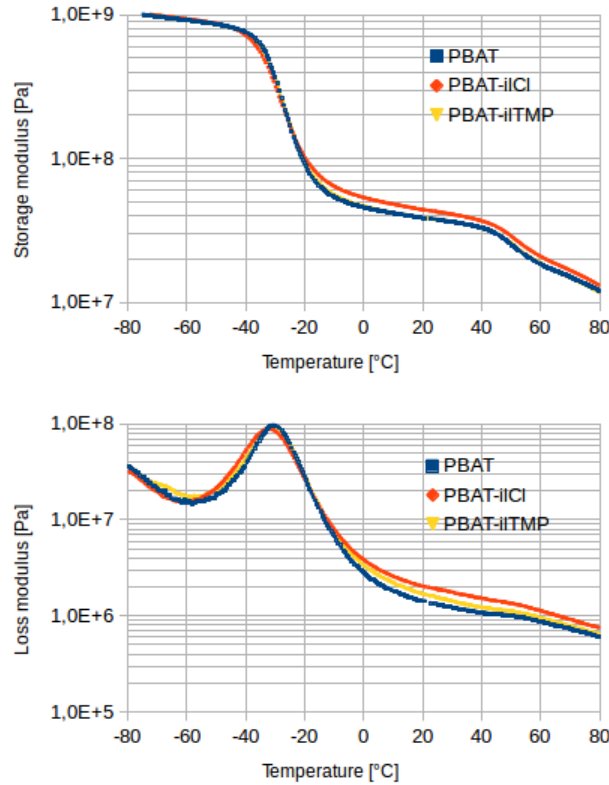


Figure 5: Variation of the storage modulus (top) and of the loss modulus (bottom) of PBAT and PBAT-ILs blends with temperature at 1 Hz

The storage modulus drop around -30°C, associated with a peak in the losses, is very likely to correspond to the α transition of the blends, passing from a glassy state at low

Table 3: Transition temperatures observed in DMA (from the loss peak) and DSC analysis. All the values are given with $\pm 1^\circ\text{C}$.

Blend:	T_α (DMA) [$^\circ\text{C}$]	T_g (DSC) [$^\circ\text{C}$]
PBAT	-30.5	-35.1
PBAT/il-Cl	-32.4	-35.0
PBAT/il-TMP	-30.8	-36.0

temperatures to a rubbery state. The α transition temperature T_α can be defined by the temperature at the maximum of the loss modulus peak.

The results are summarized in Table 3. They are in good accordance with the glass transition temperatures obtained by DSC, which also correspond well to the results reported by Livi *et al.*

No significant drop of the glass transition temperature is observed. Those results are not likely to correlate any plasticization effect induced by the ionic liquids. Even if such a slight effect is possible (-2°C in the T_α of the PBAT/il-Cl blend, but not confirmed in DSC), it cannot explain the big modifications of mechanical properties induced by the addition of 2wt% il-Cl.

A second transition can be observed on the DMA curves around 50°C , with a slight drop of both moduli. This can be associated with an α' interfacial relaxation. Since it can be observed in all the blends and not only PBAT/il-TMP, the corresponding interface is likely to be the one between the crystalline phase and the amorphous phase, and/or an amorphous interphase between crystalline lamellae, as reported in P(VDF-CTFE)⁴/ILs blends by Yang *et al.*[9].

3.1.5. Summary of the morphological, thermal and mechanical characterizations

The routine characterizations techniques described above showed that, except for the il-TMP nodules, no significant difference of the organization of the matrix is induced by the ionic liquids: the density, the crystallinity (degree and structure) and the thermal/thermo-mechanical properties remain almost unchanged by the addition of 2wt% of a ionic liquid.

⁴Poly(vinylidene fluoride-*co*-chlorotrifluoroethylene)

It is thus proposed to explore deeper the interactions between phases and within the phases, using nanomechanical data measured in AFM and dielectric spectroscopy to answer the appearing problem: how 2wt% of a ionic liquid can significantly change the mechanical properties of the matrix (increase of the strain at break with, for il-Cl, a small decrease of the Young’s modulus) without affecting the other bulk properties ?

3.2. Elucidating the mechanisms of interactions of ILs with the PBAT matrix

3.2.1. Dielectric spectroscopy and nanomechanical analysis

Dielectric spectroscopy. An example of the spectra obtained for the relative dielectric permittivity ϵ_r' and the corresponding loss ϵ_r'' at two temperatures is given in Figure 6. For all the blends, three phenomena were evidenced: the α and α' relaxations, and conductivity at low frequencies and/or high temperatures.

On the left curve, the permittivity spectra at -22°C displays a slight peak in ϵ_r'' around 100 Hz, which corresponds to the α relaxation. For PBAT/il-Cl, this peak is merged into the conduction slope, but is still identifiable. The activation energies calculated from the Havriliak-Negami fits parameters for the blends are summarized in Table 4, obtained from Arrhenius plots shown in Figure 7. Although the value of the activation energy for the alpha relaxation of PBAT/il-TMP could not be calculated properly, no major difference is expected, as between the neat PBAT and PBAT/il-Cl (less than 3%), since the corresponding relaxation occurs almost at the same temperature for all the blends, as observed in DMA and DSC.

Table 4: Activation energies (E_A) of each phenomena observed in dielectric spectroscopy. All the values are given in $kJ.mol^{-1}$

E_A of:	α relaxation	α' relaxation	Conductivity
PBAT	232.6	72.4	69.4
PBAT/il-Cl	239.0	82.8	80.7
PBAT/il-TMP	- ^b	72.4	67.0

^b This value was not calculated because the corresponding relaxation could not be fitted properly, due to overlapping phenomena (conduction) in the frequency domain.

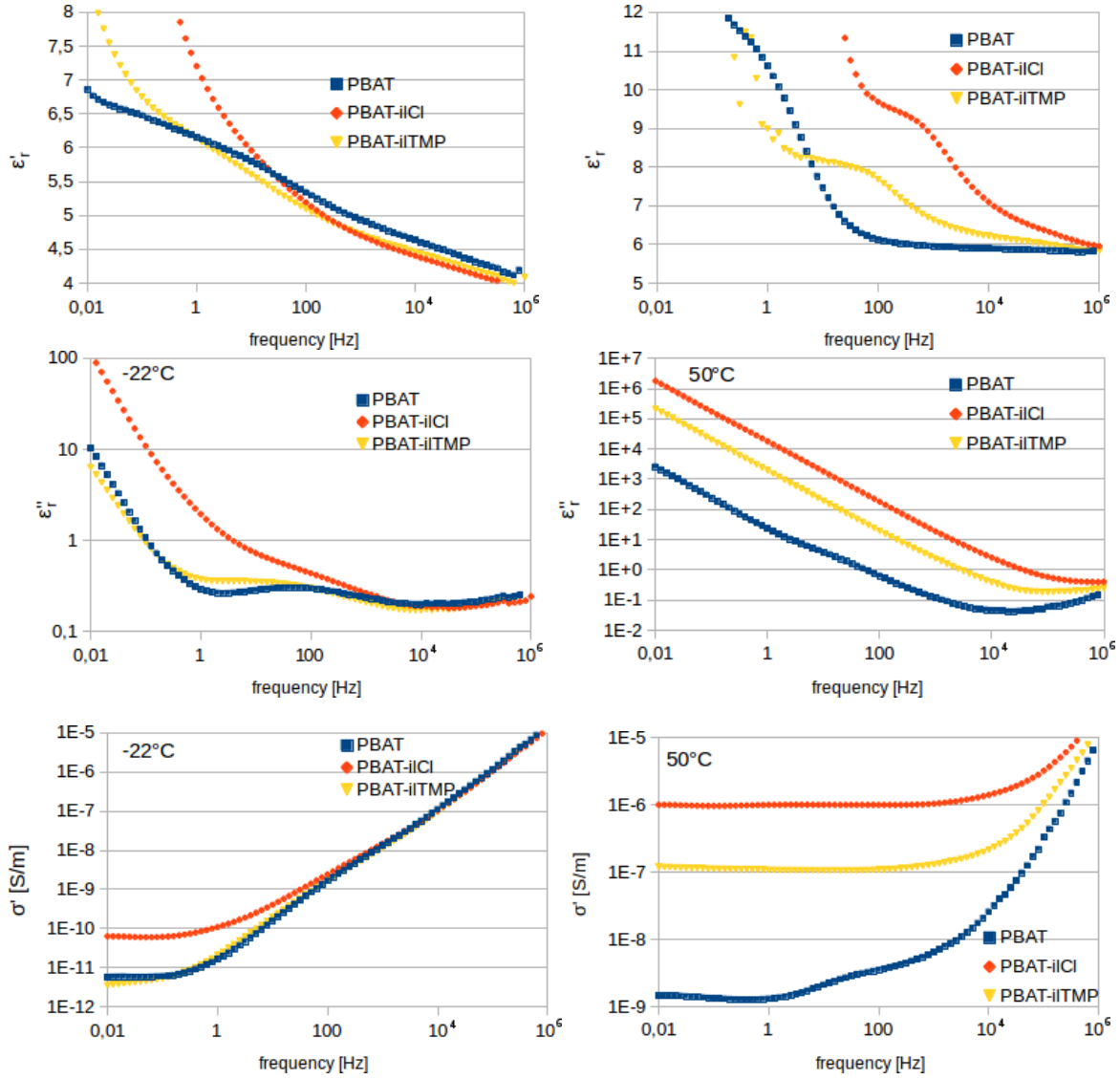


Figure 6: Relative dielectric permittivity (top), loss (middle) and real conductivity (bottom) versus frequency, at -22°C (left) evidencing the α relaxation around 100 Hz and at 50°C (right) showing conduction and the α' relaxation. The latter corresponds to the conductivity step around 100 Hz for PBAT, and is overlapped by the conduction for the other blends (It corresponds anyway to the steps in ϵ_r'' and could be fitted properly).

In the diagrams of Figure 6 (right), the real and imaginary parts of the complex permittivity of the three blends at 50°C (323 K) are shown with their frequency dependence. ϵ'' (bottom right) mostly reveals an important conduction phenomenon in the three cases, much more important for the blend with il-Cl and also relevant for the PBAT/il-TMP system. This can be explained by ionic conductivity, first induced by impurities in the PBAT matrix, and

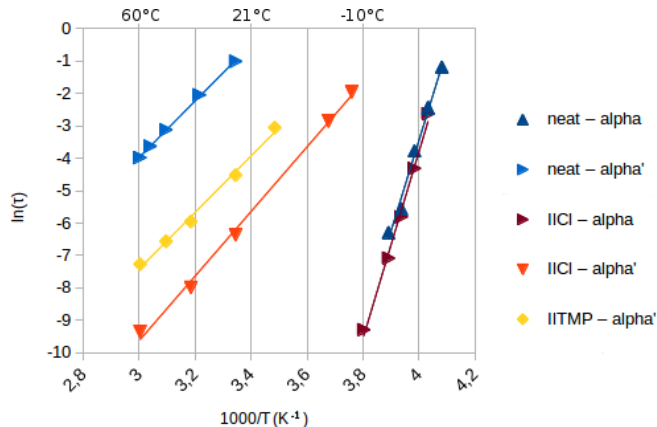


Figure 7: Arrhenius plots for the described relaxations. All linear regression fits are obtained with a squared correlation coefficient superior to 0.99. Similar results were obtained for the conductivities.

by the ionic liquids in the blends. The miscibility of il-Cl and the smaller size of the chloride anion correlates higher conduction losses for PBAT/il-Cl.

If the α' relaxation peak at 50°C is almost totally masked by the conductivity slopes in the imaginary permittivity spectrum (loss) in Figure 6, the ϵ'' spectrum (top right) reveals a step for the three systems, which corresponds to this relaxation. This may reflect the confined part of the amorphous phase, *i.e.* the chains that are confined between the crystalline lamellae or anchored in the crystalline phase, often called rigid amorphous phase or fraction (RAF)[9]. In other words, this reflects the interface between the amorphous and crystalline phases. The broadness of the corresponding loss peak in DMA and in dielectric spectroscopy, reason why it is almost masked in both cases by other phenomena, confirms this idea, as described by Alegria and Colmenero[54].

The PBAT polymer, having a relatively low crystallinity (*i.e.* between 10 and 15%[52, 34]), fits well in the category of semicrystalline polymers that are likely to form such an interfacial amorphous phase (RAF), distinct from the fully free chains of the main amorphous phase, denoted mobile amorphous fraction (MAF)[55]. Furthermore, the formation of a rigid amorphous phase was already reported for the PBT polymer[56]. The two amorphous zones can be observed in Figure 4, where dark blue domains correspond to the MAF (represented by the α relaxation) and the inter-lamellar amorphous regions (for instance the darker strips in the orange crystalline zones) correspond to the RAF (represented by the α' relaxation).

In terms of activation energy (Table 4), both ionic conductivity and α' relaxation reveal

the same trend: on one hand, those phenomena in neat PBAT and in PBAT/il-TMP seem to require the same activation energy. This is consistent with the fact that il-TMP is immiscible (or very slightly miscible) in the PBAT matrix. The same matrix is characterized for neat PBAT and PBAT/il-TMP, the nodules having almost no influence in the dielectric response, except that they increase the ionic conductivity.

On the other hand, both the conduction and the α' relaxation require around 15 to 20% more energy in the blend with 2wt% il-Cl (even if the number and size of its charge carriers make it more conductive than the other blends). The ionic liquid may thus play a role in the interfacial amorphous zone between the PBT-rich crystalline phase and the rest of the amorphous phase.

This observation for PBAT/il-Cl cannot be directly correlated with the tensile mechanical properties summarized in Figure 1: interfacial relaxation and conduction phenomena require more energy in this blend while it is mechanically softer and with a higher strain at break. This necessarily hints the coexistence of various different (but certainly interdependent) mechanisms induced by the ionic liquid. They are discussed in the following section.

Nanomechanical analysis. An AFM nanomechanical analysis was carried out over a large number of images for every system to evaluate what are the nanoscale mechanisms that explain such modifications of macroscopical properties, unexpected dielectric spectroscopy results and almost no substantial difference in other physical properties.

First, the DMT moduli from mappings such as those presented in Figure 2 were gathered into distributions. Figure 8 displays such representative diagrams for the three blends.

With the support of additional AFM nanomechanical data, a synthesis of the effects of the two different ionic liquids on the PBAT matrix are discussed in the following sections.

3.2.2. *Effect of il-TMP*

In Figure 8, the main peaks of the neat PBAT and of the PBAT/il-TMP blend are centered around 140 MPa, which correlate the fact that the continuous matrix in PBAT/il-TMP behaves similarly to the neat PBAT.

Although the reported low miscibility may limit any effect of the il-TMP on the matrix[57], in the distribution in Figure 8, the PBAT/il-TMP system also exhibit a low modulus shoulder

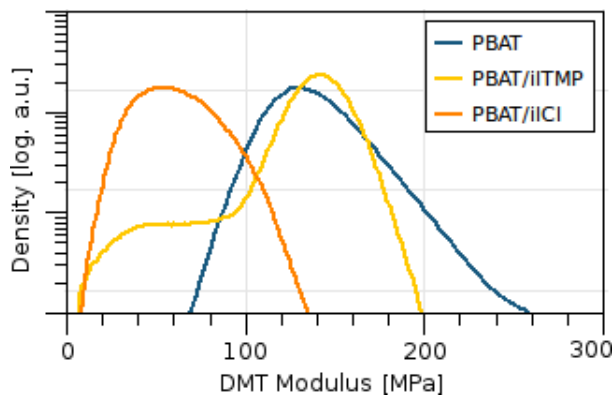


Figure 8: Representative logarithmic distributions of DMT modulus over AFM images for each blend. The vertical axis represents the density of probability associated with each modulus value in modulus mappings.

that corresponds to the softer il-TMP nodules. It is a continuous shoulder and not a distinct peak, suggesting the existence of transitional zones between ionic liquid nodules and PBAT matrix, *i.e.* an interphase.

In Figure 9, the same profile is taken across the height image and the DMT modulus image. The region between the two vertical dashed blue lines on the height profile can be interpreted as the matrix edge, close to the interface with the nodule, since there is no significant height variation with the rest of the matrix.

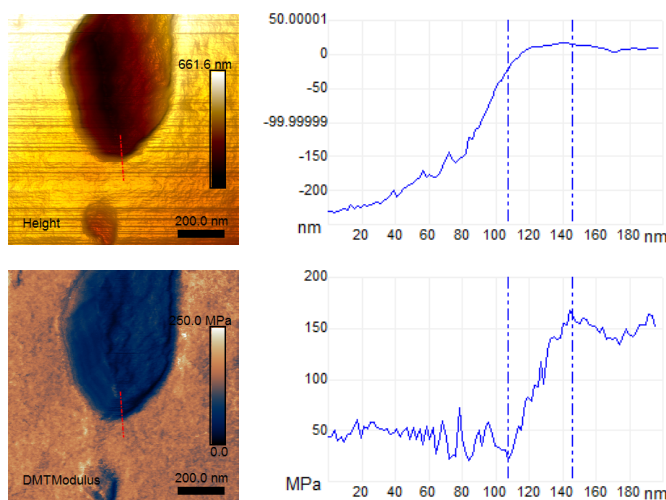


Figure 9: AFM $1 \times 1 \mu\text{m}^2$ topography (top) and DMT modulus (bottom) images of a PBAT/il-TMP surface with corresponding profiles, taken following the red dashed line.

However, in that zone of about 40 nm, a DMT modulus transition can be observed into

the polymer matrix. This can be interpreted as an interphase constituted by free dangling segments of the polymer chains from the matrix, explaining the smooth modulus transition. The neat PBAT modulus is quickly restored when going further into the matrix, due to the immiscibility of the ionic liquid.

It is known that phosphonium cation and phosphinate anions are among the most basic ions used in ionic liquids[58, 59]. Studies reports that basic ionic liquids are good catalysts for depolymerisation of polyesters structurally similar to the PBAT, for instance poly(lactic acid)[60] and polyethylene terephthalate[61, 57]. This may also affect the aspect of the interphases, but it couldn't be confirmed experimentally.

Figure 10 displays a mapping of the dissipated energy at each tip-sample contact, for the PBAT/il-TMP blend. It can be clearly observed that the nodules (or the corresponding interphases) correspond to zones where more energy can be dissipated. The macroscopical strain at break of this blend increased by 33% for this blend compared to the neat PBAT, according to Livi *et al.*[34] (This can be explained by the fact that the blend can store more energy under stress due to its IL nodules, which can hinder the crack propagation, thus increasing the strain at break while the continuous matrix keeps the Young's modulus of the neat PBAT.

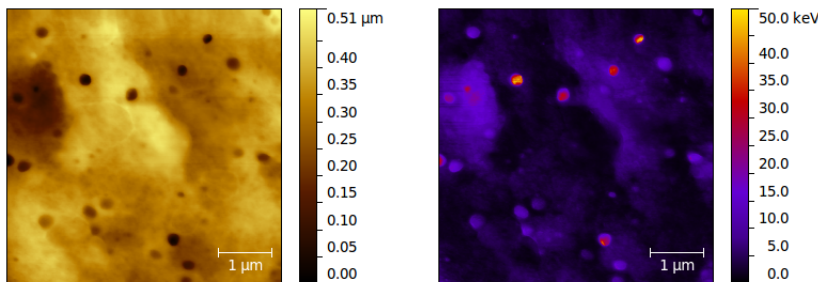


Figure 10: Topography (left) and dissipation energy (right) AFM nanomechanical mappings of the PBAT/il-TMP blend, revealing the dissipative nature of the nodules.

3.2.3. Effect of *il-Cl*

As shown in Figure 8, PBAT/*il-Cl* exhibits a DMT modulus distribution centered around 60 MPa, which is less than the half of the equivalent for the other blends. This trend is observed for all the recorded mappings. In tensile tests, the modulus drops only by 18%

with the addition of 2wt% of il-Cl, and as seen above, this cannot be only explained by a plasticization effect (no significant variation of the T_g is observed in DSC measurements). As il-Cl seems totally miscible with the matrix, an attempt to localize it can be made using adhesion mappings, as already done in a previous study on PBAT/PLA/ILs blends[33].

First, different zones of the PBAT matrix have to be identified. As seen with the XRD analysis, the crystalline phase of the PBAT matrix is composed by stiff PBT units. The amorphous phase, which is majoritary, may consist mostly in butylene adipate segments, along with the rest of the butylene terephthalate. In DMT modulus images, spherulites are easily identifiable. Finally, an intermediate amorphous phase (RAF), characterized by the α' relaxation, was also identified by dielectric spectroscopy and DMA.

In Figure 11, based on their shape, some obvious spherulites were marked in red on the DMT modulus images for PBAT/il-Cl and neat PBAT, and the mask was reported on the adhesion mappings. It is worth noting that the spherulites may not only be constituted by the crystalline phase, but also by inter-lamellar rigid amorphous zones.

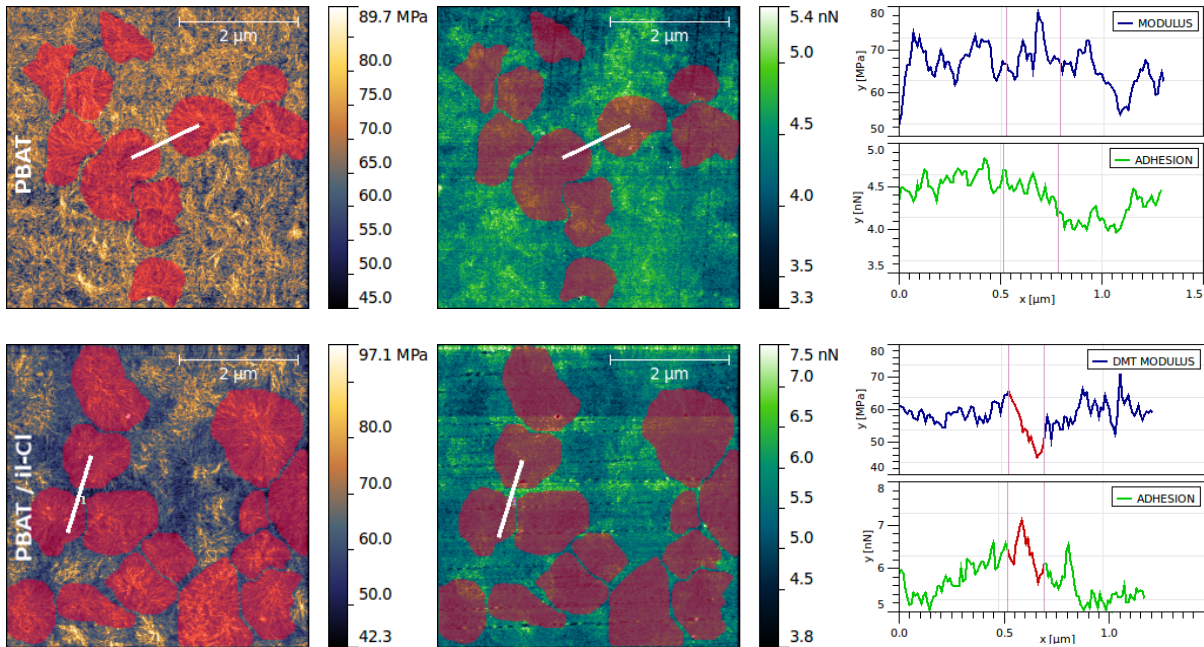


Figure 11: AFM $5 \times 5 \mu\text{m}^2$ DMT modulus (left) and adhesion (center) images with corresponding profiles (right) for neat PBAT (top) and PBAT/il-Cl (bottom). The profiles are taken following the white lines in the images, and the vertical purple lines on the profiles correspond to the gaps between zones marked in red. Some (but not all) clearly identifiable spherulites are marked in red in the images.

The crystalline zones being identified, it can be observed that PBAT and PBAT/il-Cl follow different trends:

- On the one hand, for the neat PBAT, the lamellar crystallinity seems to be the only contrast factor in the DMT modulus image. Between the purple vertical lines in the profiles in Figure 11, a zone between spherulites that corresponds to the amorphous phase, no significant difference with the rest of the profile is visible in adhesion.
- On the other hand, for the PBAT/il-Cl blend, a clear difference can be seen between zones with crystalline phase (*i.e.* spherulites, marked in red) and zones between spherulites (mainly corresponding to the MAF), that exhibits a lower local modulus and higher adhesion. This can be observed in the profiles, where the part of the curves that corresponds to the amorphous zone between spherulites is marked in dark red, displaying a modulus drop and an adhesion peak. The fact that adhesion forces reaching values that are not observed on the neat PBAT³ hints the presence of another component, *i.e.* the ionic liquid. The adhesion mappings reveal thus that il-Cl may be preferentially located in the amorphous phase of the PBAT matrix.

Based on such observations, an explanation of the complex effect of il-Cl on the PBAT matrix can be made. First, the ionic liquid, located mostly in the amorphous phase of the PBAT, tends to increase drastically the chain mobility at the nanoscale in the MAF, explaining the local (DMT) modulus drop observed in AFM, compared to that of the other systems (see Figure 8).

The il-Cl should obviously be present not only in the MAF but also in the RAF, given its effect on the α' relaxation. The polymer chains being much more constrained in this phase, the ionic liquid may act differently and reduce even more their movement capability, thus making the relaxation of this zone requiring more energy (dielectric data). This may represent a gain in stiffness at a higher scale than what is observed in AFM, counterbalancing the dramatic drop in the nanoscale modulus, explaining a lesser drop in the macroscopic

³It is worth noting that to compare adhesion forces quantitatively from an image to another, the images in Figure 11 were acquired in the same session with the same tip.

scale Young's modulus. From this point of view, the ionic liquid has the same role as a filler functionalization, but with the crystalline phase.

This can also be explained by a cooperation effect between the ions of il-Cl and the polymer chains, due to dipole-dipole and/or ionic interactions, that should be much more present than in the neat blend. These interactions are also highlighted by the conductivity data: if the conductivity is more important in the PBAT/il-Cl blend, the energy required to activate the conduction is much higher than in the other systems.

The phosphonium-chloride ionic liquid have thus a double effect on the PBAT matrix: on one hand it acts like a local plasticizer, increasing the chain mobility in the MAF phase (thus increasing the global strain at break), but on the other hand it forms strong cooperating interactions, particularly in the interfacial RAF phase, compensating some effects induced by the gain in chain mobility and limiting the Young's modulus decrease.

4. Conclusions

The effects of the introduction of a small amount (2wt%) of two different phosphonium ionic liquids on the structure and mechanical properties of a PBAT copolyester have been investigated using advanced characterization techniques, and in particular AFM nanomechanical imaging. This method allows, via the simultaneous acquisition of several images of the same surface, high resolution mappings of different mechanical properties such as the local elasticity modulus, the tip-sample adhesion force and the energy dissipation. By this way, the nanostructure of a material is explored from unusual points of view, allowing to go deeper into the understanding of the molecular organization of the studied polymers, and the way they are modified, here by ionic liquids.

The tensile mechanical properties of the PBAT matrix were affected by both ionic liquids: while the addition of a phosphonium-phosphinate ionic liquid, denoted il-TMP, increased the strain at break of the matrix by 33% without affecting the Young's modulus, the same amount of il-Cl, a phosphonium-chloride IL, increased the strain at break by 60% and reduced the modulus from 47 to 40 MPa. However, no substantial modification of the density, of the crystalline structure and of thermal properties (*i.e.* the glass transition temperature and the crystallinity) were recorded.

The same crystalline structure was identified in the three systems, consisting in lamellae constituted by PBT segments. Two amorphous phases were identified by dielectric spectroscopy according to their relaxation behavior: the mobile amorphous fraction (MAF) and the rigid amorphous fraction (RAF). The former consists in fully free polymer chains in relatively large amorphous domains while the latter represents the constrained chains between crystalline lamellae or at the crystalline/amorphous interface.

It was shown that il-TMP is immiscible in the PBAT, but organizes itself into dissipative nodules that form, as shown by profile analysis in AFM, a smooth interphase with the matrix, consisting in softer dangling polymer chains. Being continuous, the PBAT matrix keeps most of its properties while the nodules just hinders the defaults propagation under stress, increasing the strain at break. To confirm this effect macroscopically using a tearing strength test on films with and without il-TMP could be an interesting perspective, as it is directly applicable for compostable PBAT films used in agriculture.

The other ionic liquid, il-Cl, is perfectly miscible in the amorphous phases of the PBAT matrix, as observed with AFM adhesion mappings. In the MAF, the overall effect seems to be a dramatic increase of the chain mobility, explaining a huge local modulus drop (more than -50% in average) and the 60% increase in the macroscopic strain at break, with relatively free charge carriers explaining a higher conductivity than in other blends. This is partially compensated by a stiffening effect of the ionic liquid on the RAF, as it increases the activation energy associated with the relaxation of this phase. The ionic liquid has thus a double effect, allowing to optimize the mechanical properties (the macroscopic Young's modulus is only reduced by 20%) and to keep unchanged the crystalline structure and the glass transition temperature.

Through the example of PBAT, this study highlights the potential of ionic liquids, whose structuring effect could be an alternative to traditional additives to tailor and tune the properties of polymers. According to the desired modification of the properties, at least three possibilities can be identified with ionic liquids:

- A traditional plasticization effect, as reported for instance by Sankri *et al.* with an imidazolium ionic liquid on a starch matrix[2]. This would mean an increase of the strain at break, and a decrease of the Young's modulus and of the glass transition

temperature.

- An increase of the strain at break with a moderate decrease of the Young's modulus, but without affecting the thermal properties, as reported for the blend with il-Cl.
- An increase of the strain at break without affecting much the modulus, as reported for the blend containing il-TMP.

The combination of AFM nanomechanical mappings with other advanced characterization techniques such as dielectric spectroscopy allowed to access complex structuring mechanisms that link mechanical, thermal and electric properties together, allowing to explain the influences of ionic liquids on the properties of a polymer matrix.

Acknowledgements

The authors acknowledge the French *Ministère de l'Enseignement Supérieur et de la Recherche (MESR)* and *École Doctorale Matériaux* for supporting this project. They also thank R. Vera from the *Centre de Diffraction H. Longchambon* (UCBL) for the XRD experiments, and P. Alcouffe (UMR5223) for the surface preparation of AFM samples.

References

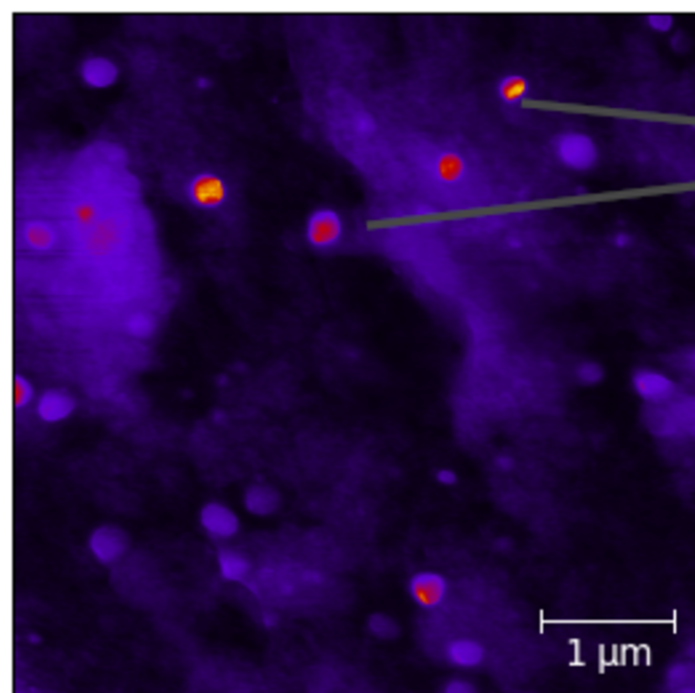
- [1] J. Lu, F. Yan and J. Texter, *Progress in Polymer Science*, 2009, **34**, 431–448.
- [2] A. Sankri, A. Arhaliass, I. Dez, A. C. Gaumont, Y. Grohens, D. Lourdin, I. Pillin, A. Rolland-Sabaté and E. Leroy, *Carbohydrate Polymers*, 2010, **82**, 256–263.
- [3] K. Park and M. Xanthos, *Polymer Degradation and Stability*, 2009, **94**, 834–844.
- [4] B.-K. Chen, T.-Y. Wu, Y.-M. Chang and A. F. Chen, *Chemical engineering journal*, 2013, **215**, 886–893.
- [5] R. P. Swatloski, S. K. Spear, J. D. Holbrey and R. D. Rogers, *Journal of the American chemical society*, 2002, **124**, 4974–4975.
- [6] S. Livi, V. Bugatti, L. Estevez, J. Duchet-Rumeau and E. P. Giannelis, *Journal of colloid and interface science*, 2012, **388**, 123–129.

- [7] L. C. Lins, S. Livi, J. Duchet-Rumeau and J.-F. Gerard, *RSC Adv.*, 2015, **5**, 59082–59092.
- [8] T. K. L. Nguyen, S. Livi, S. Pruvost, B. G. Soares and J. Duchet-Rumeau, *Journal of Polymer Science Part A: Polymer Chemistry*, 2014, **52**, 3463–3471.
- [9] J. Yang, S. Pruvost, S. Livi and J. Duchet-Rumeau, *Macromolecules*, 2015, **48**, 4581–4590.
- [10] G. Binnig, C. F. Quate and C. Gerber, *Physical Review Letters*, 1986, **56**, 930–933.
- [11] I. Siretanu, J. P. Chapel and C. Drummond, *ACS nano*, 2011, **5**, 2939–2947.
- [12] Q. Zhong, D. Inniss, K. Kjoller and V. Elings, *Surface Science Letters*, 1993, **290**, L688–L692.
- [13] M. R. Vanlandingham, S. H. McKnight, G. R. Palmese, J. R. Elings, X. Huang, T. A. Bogetti, R. F. Eduljee and J. W. G. Jr., *The Journal of Adhesion*, 1997, **64**, 31–59.
- [14] M. Radmacher, M. Fritz, C. M. Kacher, J. P. Cleveland and P. K. Hansma, *Biophysical journal*, 1996, **70**, 556–567.
- [15] Bruker Corporation, *PeakForce QNM User Guide (Revision E)*, 2011.
- [16] T. J. Young, M. A. Monclus, T. L. Burnett, W. R. Broughton, S. L. Ogini and P. A. Smith, *Measurement Science and Technology*, 2011, **22**, 125703.
- [17] L. Picas, P.-E. Milhiet and J. Hernández-Borrell, *Chemistry and physics of lipids*, 2012, **165**, 845–860.
- [18] D. Wang, T. P. Russell, T. Nishi and K. Nakajima, *ACS Macro Letters*, 2013, **2**, 757–760.
- [19] D. Wang, K. Nakajima, F. Liu, S. Shi and T. P. Russell, *ACS nano*, 2017, **11**, 8660–8667.
- [20] Z. Qu, J. Bu, X. Pan and X. Hu, *Journal of Polymer Research*, 2018, **25**, 138.
- [21] S. S. Banerjee, A. Janke, U. Gohs, A. Fery and G. Heinrich, *European Polymer Journal*, 2017, **88**, 221–230.

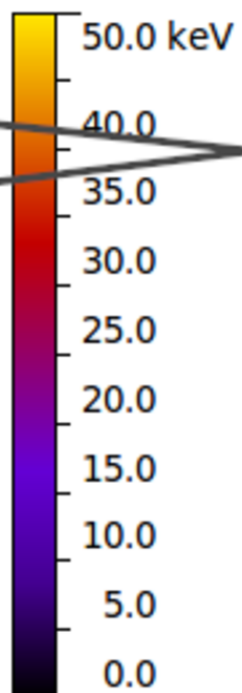
- [22] G. Mertz, F. Hassouna, P. Leclère, A. Dahoun, V. Toniazzo and D. Ruch, *Polymer degradation and stability*, 2012, **97**, 2195–2201.
- [23] S. Maruyama, Y. Ohsawa, R. Takahashi and Y. Matsumoto, *European Polymer Journal*, 2018.
- [24] Z. Chao, B. P. Radka, K. Xu, G. M. Crouch, D. Han, D. B. Go, P. W. Bohn and S. K. Fullerton-Shirey, *Small*, 2018, **14**, 1802023.
- [25] X. Shi, H. Ito and T. Kikutani, *Polymer*, 2005, **46**, 11442–11450.
- [26] J. S. P. da Silva, J. M. F. da Silva, B. G. Soares and S. Livi, *Composites Part B: Engineering*, 2017, **129**, 117–123.
- [27] Y. Nabar, J. M. Raquez, P. Dubois and R. Narayan, *Biomacromolecules*, 2005, **6**, 807–817.
- [28] M. Kumar, S. Mohanty, S. Nayak and M. R. Parvaiz, *Bioresource Technology*, 2010, **101**, 8406 – 8415.
- [29] S. Mohanty and S. Nayak, *Journal of Polymers and the Environment*, 2012, **20**, 195–207.
- [30] S. Livi, G. Sar, V. Bugatti, E. Espuche and J. Duchet-Rumeau, *RSC Adv.*, 2014, **4**, 26452–26461.
- [31] S. Livi, L. C. Lins, G. Sar, J.-F. Gérard and J. Duchet-Rumeau, *ACS Sustainable Chemistry & Engineering*, 2015, **4**, 461–470.
- [32] S. Livi, V. Bugatti, M. Marechal, B. G. Soares, G. M. O. Barra, J. Duchet-Rumeau and J.-F. Gerard, *RSC Adv.*, 2015, **5**, 1989–1998.
- [33] B. Megevand, S. Pruvost, L. C. Lins, S. Livi, J.-F. Gérard and J. Duchet-Rumeau, *RSC Advances*, 2016, **6**, 96421–96430.
- [34] S. Livi, V. Bugatti, B. G. Soares and J. Duchet-Rumeau, *Green Chemistry*, 2014, **16**, 3758–3762.

- [35] J. Odent, P. Leclère, J.-M. Raquez and P. Dubois, *European Polymer Journal*, 2013, **49**, 914–922.
- [36] J. Odent, J.-M. Raquez, P. Leclère, F. Lauro and P. Dubois, *Polymers for Advanced Technologies*, 2015, **26**, 814–822.
- [37] D. M. Panaitescu, A. N. Frone and C. Nicolae, *European Polymer Journal*, 2013, **49**, 3857 – 3866.
- [38] W. Fam, J. Mansouri, H. Li and V. Chen, *Journal of Membrane Science*, 2017, **537**, 54–68.
- [39] P. Xavier and S. Bose, *Macromolecules*, 2016, **49**, 1036–1048.
- [40] B. Derjaguin, V. Muller and Y. Toporov, *Journal of Colloid and Interface Science*, 1975, **53**, 314 – 326.
- [41] K. L. Johnson, K. Kendall and A. D. Roberts, *Proceedings of the Royal Society of London A: Mathematical, Physical and Engineering Sciences*, 1971, **324**, 301–313.
- [42] D. Maugis, *Journal of Colloid and Interface Science*, 1992, **150**, 243 – 269.
- [43] D. Dugdale, *Journal of the Mechanics and Physics of Solids*, 1960, **8**, 100 – 104.
- [44] M. Wojdyr, *Journal of Applied Crystallography*, 2010, **43**, 1126–1128.
- [45] D. Wu, L. Wu, G. Yu, B. Xu and M. Zhang, *Polymer Engineering & Science*, 2008, **48**, 1057–1067.
- [46] N. Oburoğlu, N. Ercan, A. Durmus and A. Kaşgöz, *Journal of Applied Polymer Science*, 2012, **123**, 77–91.
- [47] J. I. Langford and A. Wilson, *Journal of Applied Crystallography*, 1978, **11**, 102–113.
- [48] M. Yokouchi, Y. Sakakibara, Y. Chatani, H. Tadokoro, T. Tanaka and K. Yoda, *Macromolecules*, 1976, **9**, 266–273.
- [49] I. Hall and M. Pass, *Polymer*, 1976, **17**, 807–816.

- [50] S. Havriliak and S. Negami, *Polymer*, 1967, **8**, 161–210.
- [51] R. Briber and E. Thomas, *Polymer*, 1985, **26**, 8–16.
- [52] R. Herrera, L. Franco, A. Rodríguez-Galán and J. Puiggali, *Journal of Polymer Science Part A: Polymer Chemistry*, 2002, **40**, 4141–4157.
- [53] K. Kuwabara, Z. Gan, T. Nakamura, H. Abe and Y. Doi, *Biomacromolecules*, 2002, **3**, 390–396.
- [54] A. Alegria and J. Colmenero, *Soft matter*, 2016, **12**, 7709–7725.
- [55] B. Wunderlich, *Progress in Polymer Science*, 2003, **28**, 383–450.
- [56] S. Z. Cheng, R. Pan and B. Wunderlich, *Macromolecular Chemistry and Physics*, 1988, **189**, 2443–2458.
- [57] H. Wang, Z. Li, Y. Liu, X. Zhang and S. Zhang, *Green Chemistry*, 2009, **11**, 1568–1575.
- [58] A. F. M. Claudio, L. Swift, J. P. Hallett, T. Welton, J. A. P. Coutinho and M. G. Freire, *Phys. Chem. Chem. Phys.*, 2014, **16**, 6593–6601.
- [59] S. Spange, R. Lungwitz and A. Schade, *Journal of Molecular Liquids*, 2014, **192**, 137 – 143.
- [60] X.-Y. Li, Q. Zhou, K.-K. Yang and Y.-Z. Wang, *Chemical Papers*, 2014, **68**, 1375–1380.
- [61] Q. Yue, C. Wang, L. Zhang, Y. Ni and Y. Jin, *Polymer Degradation and Stability*, 2011, **96**, 399 – 403.

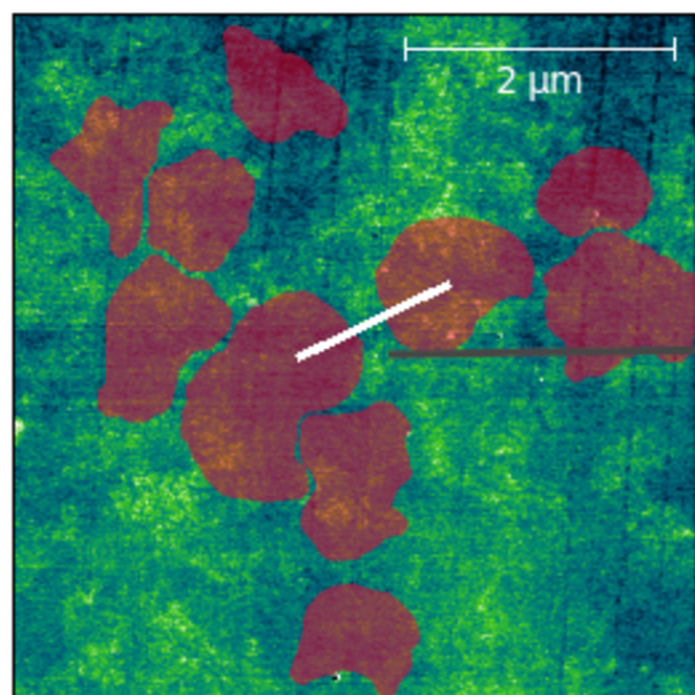


dissipation

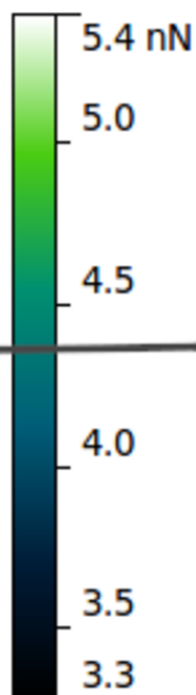


il-TMP

immiscible
dissipative
nodules



adhesion



il-CI

miscible in
amorphous
phase